

# PolarTracker: Attitude-Aware Channel Access for Floating Low Power Wide Area Networks

Yuting Wang<sup>ID</sup>, Xiaolong Zheng<sup>ID</sup>, Member, IEEE, Liang Liu<sup>ID</sup>, Member, IEEE,  
and Huadong Ma<sup>ID</sup>, Fellow, IEEE

**Abstract**—Low Power Wide Area Networks (LPWAN) such as Long Range (LoRa) show great potential in emerging aquatic IoT applications. However, our deployment experience shows that the floating LPWAN suffers significant performance degradation, compared to the static terrestrial deployments. Our measurement results reveal the reason behind this is the polarization and directivity of the antenna. The dynamic attitude of a floating node incurs varying signal strength losses, which is ignored by the attitude-oblivious link model adopted in most of the existing methods. When accessing the channel at a misaligned attitude, packet errors can happen. In this paper, we propose an attitude-aware link model that explicitly quantifies the impact of node attitude on link quality. Based on the new model, we propose *PolarTracker*, a novel channel access method for floating LPWAN. *PolarTracker* tracks the node attitude alignment state and schedules the transmissions into the aligned periods with better link quality. To support concurrent access of multiple LoRa nodes, an attitude-based slotted-ALOHA protocol is proposed to reduce collision. We implement a prototype of *PolarTracker* on commercial LoRa platforms and extensively evaluate its performance in various real-world environments. The experimental results show that *PolarTracker* can efficiently improve the packet reception ratio by 50.6%, compared with ALOHA in LoRaWAN.

**Index Terms**—Floating LPWAN, attitude-aware, channel access, aquatic environments.

## I. INTRODUCTION

DESPITE the prosperity of the Internet of Things (IoT) in terrestrial environments including both urban and rural areas, its applications in aquatic environments remain scarce. With the development of Low Power Wide Area Networks (LPWAN) such as LoRa (Long Range) [1], [2], IoT systems begin to be deployed in aquatic environments such as oceans [3], [4], reservoirs [5], and rivers [6]. The nodes equipped with anchors float on the water surface, forming

Manuscript received June 16, 2021; revised December 1, 2021 and February 13, 2022; accepted February 14, 2022; approved by IEEE/ACM TRANSACTIONS ON NETWORKING Editor F. Dressler. This work was supported in part by the Funds for Creative Research Groups of China under Grant 61921003, in part by the National Natural Science Foundation of China (NSFC) under Grant 62072050, in part by the A3 Foresight Program of NSFC under Grant 62061146002, in part by the Fundamental Research Funds for the Central Universities under Grant 2019XD-A14, and in part by the Beijing University of Posts and Telecommunications (BUPT) Excellent Ph.D. Students Foundation under Grant CX2021309. (Corresponding authors: Xiaolong Zheng; Liang Liu.)

The authors are with the Beijing Key Laboratory of Intelligent Telecommunication Software and Multimedia, Beijing University of Posts and Telecommunications, Beijing 100876, China (e-mail: wangyuting@bupt.edu.cn; zhengxiaolong@bupt.edu.cn; liangliu@bupt.edu.cn; mhd@bupt.edu.cn).

Digital Object Identifier 10.1109/TNET.2022.3154937

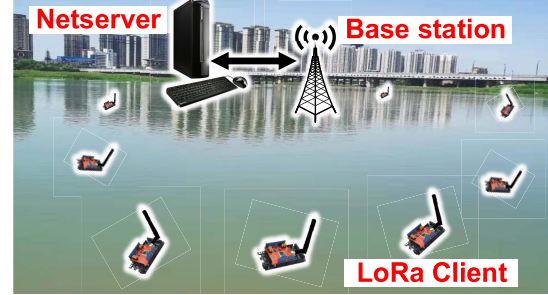


Fig. 1. LoRaWAN architecture.

the so-called floating LPWAN, as shown in Fig. 1. LoRa improves the sensitivity by Chirp Spread Spectrum (CSS) modulation. For example, Semtech chipset SX1278 [7] claims a -148 dBm sensitivity. Such a high sensitivity can extend the communication range and offer good reliability, showing great potential in floating IoT deployments.

However, in practice, we surprisingly observe a significant performance degradation when migrating the LoRa deployment from the land to the water. In an open water area, with the transmission power (Tx power) of 4 dBm, a floating node 0.3km away from the gateway can only achieve a Packet Reception Ratio (PRR) of 64.7%, whereas the terrestrial node at the same distance can obtain 84% PRR. During the experiments, we also observe more violent node sway with a larger magnitude leads to the more severe PRR degradation.

Our further measurement reveals that the reason behind the performance degradation is the attitude-oblivious channel access mechanism inherited from the terrestrial system designs. The antenna of the floating node will change with its attitude, which further brings about the polarization misalignment of the transceiver antennas. The polarization misalignment will affect the transmission efficiency of the signal. The existing attitude-oblivious link model neglects the non-trivial impact of attitude on the link quality and allows channel access immediately when the transmitter has a packet. The ignorance is unproblematic in terrestrial networks because their nodes usually don't have sharp attitude changes. But for a floating node, the constantly changing attitude will lead to the dynamic additional signal attenuation, resulting in unstable PRR.

How to get reliable performance for the floating LPWAN is still an open problem. Adopting more robust LoRa parameters such as increasing the Tx power or coding rate [8], [9] will lead to poor energy efficiency. For floating networks in open

water, energy is often carefully planned without a redundant budget. On the other hand, blind retransmissions [10], [11] consume too much energy but obtain limited improvements because the retransmission can still happen at the misaligned attitude. In a nutshell, these conventional reliability enhancement methods are inefficient because they rely on the attitude-oblivious link model and fail to capture the short-term link quality variations caused by the fast-changing attitude.

To tackle the above problem, a channel access method that can capture the best-aligned attitude is desired. But getting such a method faces the following challenges. First, though we know the polarization misalignment causes signal strength loss, the relationship between the link quality and the floating attitude is still unclear. Besides, the antenna directivity further complicates the relationship. Blurring the impact of attitude on link quality inevitably incurs errors in seizing the channel access opportunities. Second, pinpointing the best channel access timing is challenging in practice. Channel probing is infeasible because the LoRa's long packet transmission time results in a too low probing rate to timely detect the fast-changing link quality. The floating node can sway a wide magnitude within one second. But a LoRa packet can take tens of milliseconds and even seconds, leaving too many undetected attitudes and therefore missing the best opportunity. Third, when designing the channel access methods for the floating LPWAN that desire a long lifetime to reduce the maintenance cost, low power consumption should always be kept in mind.

By settling these challenges, we propose *PolarTracker*, an attitude-aware channel access method for the floating LPWAN.

- By thoroughly exploiting antenna polarization and directivity, we conduct real-world observation and discover the relationship between node attitude and signal strength loss. We further propose an attitude-aware link quality model to explicitly quantify the impact of node attitude on link quality, which is a fundamental model that can guide the following system designs in aquatic environments.
- We propose *PolarTracker*, a novel channel access method for the floating LPWAN. *PolarTracker* tracks the dynamic node attitude alignment state and schedules packets into the aligned periods to obtain better link quality. To the best of our knowledge, *PolarTracker* is the first work that discovers and resolves the reliability problem of LPWAN caused by the dynamic attitude in aquatic environments.
- To support concurrent access of multiple LoRa nodes with the same best-aligned period, an attitude-based slotted-ALOHA protocol is proposed. *PolarTracker* achieves effective access of multiple nodes by adjusting the transmission slots dynamically and adaptively according to the dynamic attitude.
- We implement a prototype of *PolarTracker* and extensively evaluate its performance in real-world scenarios. Our evaluation results show that *PolarTracker* can accurately track the aligned attitude and improve the PRR by  $1.48\times$ , compared to ALOHA used in LoRaWAN.

The rest of this paper is organized as follows. We discuss the related works in Section II. Section III introduces the background and our measurement of a floating LoRa network,

which motivates our work. We then propose the attitude-aware link quality model in Section IV and present the designs of *PolarTracker* in Section V. Evaluation results are shown in Section VI and finally we conclude this paper in Section VII.

## II. RELATED WORK

**WSNs in Aquatic Environments:** Despite the prosperity of IoT in terrestrial environments [12]–[15], its applications in aquatic environments remain scarce. But researchers keep attempting to apply IoT in aquatic environments for many years. The early deployments mainly use short-range wireless techniques [16], [17], such as ZigBee in Oceansense [18], WiFi and LTE in [19]. But either the limited communication range or high cost of infrastructure hinders large-scale applications. The emergence of LPWAN brings to light for the floating IoT systems, due to their low cost and long communication range. In recent years, a lot of applications in aquatic environments are proposed [3]–[6].

**LoRa Reliability Improvement:** LoRa with high sensitivity is expected to have good reliability. However, according to our deployment experience, we find the reliability degradation of the floating LoRa network, which has not been discovered and solved. Existing reliability improvement methods used in territorial environments are inefficient to solve this problem. Many existing works focus on controlling the transmission parameters [8], [9], [20] to obtain better PRR but ignore the fact that using more robust parameters can cause unaffordable energy overhead for floating deployments. Similarly, blind retransmissions [10], [11] consume too much energy but obtain limited improvements. Moreover, a few MAC protocols are proposed to balance loads of the channels defined by frequencies and spreading factors [21]. Different from the existing works, we focus on exploring the impact of variable polarization matching state on reliability caused by the dynamic attitude of the floating nodes in aquatic environments.

**Polarization Matching in Traditional Wireless:** Polarization mismatch due to dynamic attitude is a traditional problem in wireless. In LTE, dual-polarized antennas with high gain are usually used to reduce the effect of polarization mismatch [22], [23]. For example, in [22], a dual-band dual-polarized planar array with a flat-top and sharp-cutoff radiation pattern for base stations is proposed to improve the radiation characteristics. Circularly polarized antennas are widely used in RFID readers because they can reduce the loss caused by polarization mismatch. In [24], a circularly polarized (CP) V-shaped patch antenna is proposed for RFID application. Moreover, for RFID, new types of tags are designed to reduce polarization mismatch issues, such as a miniature omnidirectional tag in [25], a two-tag array labeled RFID system [26].

However, the above methods are in the terrestrial environment with small attitude variation, while for floating LPWAN, the antenna attitude changes rapidly and violently. In addition, the communication of RFID and LTE requires high SNR and the problem of polarization mismatch is not prominent. LoRa with low sensitivity reception characteristics is usually used in long-distance communication with low SNR, which is more affected by polarization mismatch. Moreover, for such low-power devices, the loss of  $3dB$  using a circularly polarized

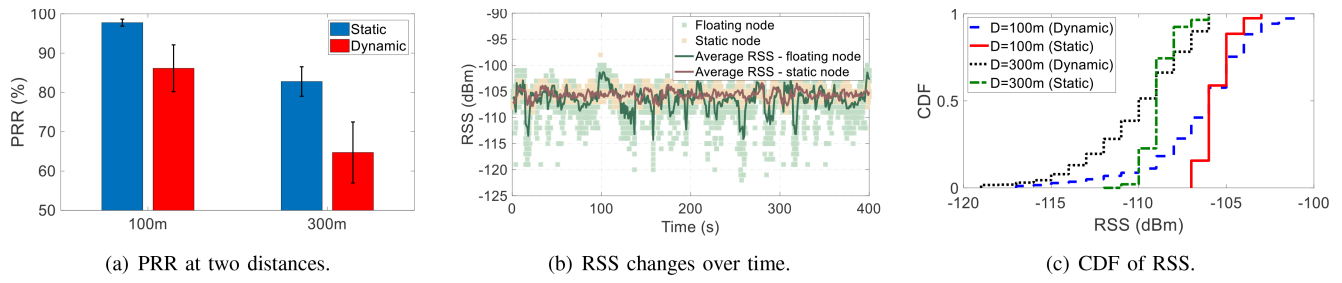


Fig. 2. The measurement results of the existing method in static and floating environments.

antenna is inefficient. Our work for the first time explicitly addresses the LoRa transmission reliability using such polarization matching state caused by the dynamic attitude of the floating nodes.

### III. BACKGROUND AND MOTIVATION

In this section, we first briefly introduce the background knowledge and then present the observations of performance degradation when applying LoRa in aquatic environments.

#### A. Introduction of LoRa and LoRaWAN

LoRa adopts CSS modulation that signal sweeps the whole Bandwidth (BW) and forms a chirp. Spreading Factor (SF) will determine how spread out the chirp is. A larger SF leads to a longer chirp. With other parameters remaining unchanged, every increment of SF will double the transmission time of a chirp. Coding Rate (CR) indicates the used redundancy of forwarding error correction code. CR 4/5 means a one-bit correction code is added for every four data bits. Transmission power (Tx power) is another important parameter, especially for the floating LoRa networks that demand a long lifetime.

LoRaWAN [1], [27], proposed by the LoRa Alliance, defines a LoRa system architecture and the MAC protocol. LoRaWAN uses the star topology that clients directly transmit data to one or more gateways. LoRaWAN specifies three classes of the MAC protocol, based on the pure ALOHA [28]; that is, LoRaWAN clients will start transmission without any carrier sensing whenever there is a packet.

#### B. Reliability Degradation of the Floating LoRa Network

To study the performance of floating LoRa, we deploy a LoRa network in a river crossing the suburb area of a city. Two nodes are deployed on the water surface and the gateway is on a bridge 6m above the river. The horizontal distances between the gateway and two nodes are 100m and 300m, respectively. The nodes transmit packets with the Tx power of 4 dBm, using the settings of SF 7, BW 250kHz, and CR 4/5. We measure and compare the PRR of floating nodes and the close-by static terrestrial nodes with the same distance to the gateway.

The PRR results are shown in Fig. 2(a). We surprisingly find that at both distances, the PRR of floating nodes experiences obvious degradation, which is up to 64.7% at 300m. Since the only difference between the two experiments is floating nodes sway with the wave, we suspect the dynamic node attitude

influences the link quality. To verify our hypothesis, we let the floating and static nodes at 100m continuously transmit packets to the gateway and record the corresponding Received Signal Strength (RSS) no matter the packet has bit errors or not. From the results in Fig. 2(b), we can find that the RSS of the floating node has much larger variations, which can be up to 14 dBm. Given such a big RSS drop, it is no wonder the floating node's PRR degrades. In our measurement study, it is not uncommon to encounter RSS drops. From Fig. 2(c), we can find that at both distances, more than 50% of the packets experience obvious RSS degradation.

In the meantime, from the results in Fig. 2(b) and (c), we also observe the phenomenon that floating nodes obtain comparable and even larger RSS. This observation indicates there are still good transmission opportunities when the node attitude varies. However, the existing attitude-oblivious link model fails to discover and seize those opportunities. This motivates us to explore a new attitude-aware link model and design the corresponding channel access method to solve the reliability degradation problem in the floating LPWAN.

### IV. ATTITUDE-AWARE LINK MODEL

To discover and seize the good transmission opportunities, an attitude-aware link model that can quantitatively describe the impact of attitude on link quality is a foremost prerequisite. In this section, by studying the root causes of link quality reduction, we propose the corresponding attitude-aware link model for floating LPWAN.

As we all know, the signal propagates in the air will experience attenuation. The received signal strength  $P_r$  can be described by Friis Transmission Formula [29], i.e.,

$$P_r = P_t \frac{G_t G_r \lambda^2}{(4\pi d)^2} \quad (1)$$

where  $\lambda$  is the signal wavelength,  $d$  is the distance between the transceiver,  $G_t$  and  $G_r$  respectively indicate the gains of the transceiver antennas. Friis formula is widely used to analyze communication range and guide the deployments for terrestrial wireless systems.

When reviewing Eq. (1), we notice a fact that the basic Friis formula doesn't explicitly take the transceiver attitude into consideration. However, as shown in Fig. 3, the antennas used in practice are polarized and the electric field has direction. When the receiver antenna deviates the orientation aligned on the electric field, additional signal strength loss will happen. Actually, the basic Friis formula in Eq. (1) has an implicit

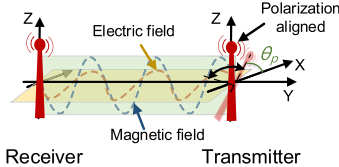


Fig. 3. Illustration of antenna polarization.

assumption that polarization between transceiver antennas is aligned. However, in the floating LPWAN, the ever-changing attitude causes the dynamic polarization alignment state. When the transmission happens at the misaligned attitude, additional signal strength loss will cause the RSS to drop. Due to the fast-changing attitude, the floating node will experience dynamic drops of RSS and PRR, as observed in Section III.

#### A. Polarization

The above analysis reveals that the dynamic polarization alignment state caused by an ever-changing attitude is the root cause of PRR degradation of the floating networks. Hence, we try to build the attitude-aware link model based on polarization and include the polarization state into the Friis formula:

$$P_r(\theta_p) = P_t \frac{G_t G_r \lambda^2}{(4\pi d)^2} p \quad (2)$$

where  $p$ , Polarization Loss Factor (PLF) [30], [31], is:

$$p = |\vec{e}_r^* \cdot \vec{e}_t|^2 = |(\cos \theta_p \vec{x} + \sin \theta_p \vec{z}) \cdot \vec{z}|^2 = \sin^2 \theta_p \quad (3)$$

where  $\theta_p$  is the polarization angle between transmitter antenna and the X-axis and  $(.)^*$  indicates the complex conjugate,  $\vec{e}_r^*$  and  $\vec{e}_t$  are respectively the unit vector of receiver and transmitter antennas. Based on the Reciprocity Theorem of antennas, the transmitting and receiving antenna beams are the same. Hence, without losing generality, the gateway antenna is regarded as vertically upward and we only consider the state of the transmitter antenna.

To verify our model, we conduct experiments with controlled attitudes. For the convenience of controlling attitude, the experiments are done in an open area on the land. We deploy a client 300m away from a base station in the same horizontal plane and rotate its antenna along the X-Z plane, as shown in Fig. 3. The client uses the setting of SF 7, BW 250kHz, and CR 4/5. The Tx power is set to 8 dBm. We reform the received power in Eq. (2) into RSS (dBm) form, which is  $RSS(\theta_p) = 10 \lg(P_r(\theta_p)) = RSS(\pi/2) + 10 \lg(\sin^2(\theta_p))$ , where  $RSS(\pi/2)$  is the signal strength when the transceiver's antenna polarizations are aligned. From Fig. 4, we can find the measured RSS fit the proposed model well at different polarization angles.

However, when we apply this model to the deployed floating network, we find packets transmitted at the aligned polarization angle ( $\theta_p = 90^\circ$ ) still get lost. Considering the floating node in the three-dimensional (3D) space also sways in the Y-Z plane, we further measure the PRR when the transceiver antenna tilts different angles in the Y-Z plane. According to the model, when we keep the polarization aligned, we should observe no obvious performance difference. However, from the

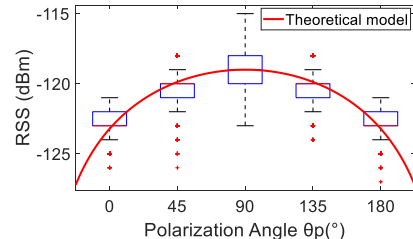
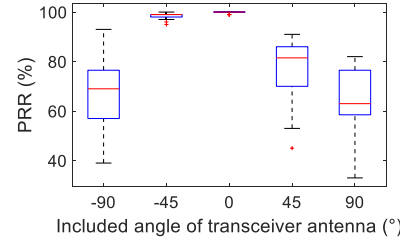
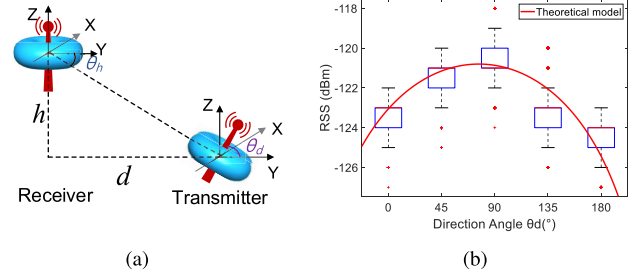


Fig. 4. RSS at different polarization angles.

Fig. 5. PRR when the client is swayed in the Y-Z plane ( $\theta_p = 90^\circ$ ).Fig. 6. Link model when considering antenna directivity with a height difference between the transceiver: (a) Illustration of the antenna directivity, where  $\theta_d$  and  $\theta_h$  are the directivity angle and the depression angle; (b) RSS at different directivity angles when the depression angle is fixed.

measured results in Fig. 5, we can clearly find PRR gaps at different angles. Besides, with the same angle deviation, tilting backwards has better PRR than tilting forwards. For example, the average PRR is 98% at  $-45^\circ$  but only 77% at  $+45^\circ$ . The observations indicate that besides polarization, there is another factor of attitude affecting the link quality.

#### B. Directivity

By analyzing the antenna design, we find that the commonly used antenna on IoT devices is the omnidirectional dipole antenna, which has directivity. Directivity is the measure of the concentration of an antennas' radiation pattern in a particular direction. The higher the directivity, the more concentrated or focused is the beam radiated by an antenna. A higher directivity also means that the beam will travel further. Instead of spherical radiation, the antenna has a toroidal radiation pattern in 3D space, as shown in Fig. 6(a). The toroidal radiation leads to very little power over and above the antenna. Hence, when there is a height difference between the transceivers, the corresponding depression angle ( $\theta_h$  in Fig. 6(a)) will incur the directional loss of the received signal strength. The swaying in the Y-Z plane will cause angular variations and exacerbate the loss. When the maximum directivity of the transceiver

antennas is perpendicular to each other, the weak signal energy can barely reach the receiver.

Hence, in the attitude-aware link model, we should take both the polarization and the directivity of the antenna into consideration. For the Friis formula in Eq. (2), we reform  $G_t$  and  $G_r$  into  $\eta_t D_t$  and  $\eta_r D_r$ , where  $\eta_t$  and  $\eta_r$  are the transceiver antenna efficiency decided by the hardware,  $D_t$  and  $D_r$  are directivity factors of the transmitter and receiver antennas. The directivity factor [30] is antenna gain in the forward direction divided by the gain in all directions for the omnidirectional antenna, which can be expressed as:

$$D(\theta) = \frac{2f^2(\theta)}{\int_0^\pi f^2(\theta) \sin \theta d\theta} \quad (4)$$

where  $\theta$  represents the angle between the antenna and the direction connecting the transceiver. For the whip antenna used in our application,  $f(\theta) = \sin(\theta)$ . Since the denominator is definite integral,  $D$  equals  $a \sin^2(\theta)$ , where  $a$  is a factor decided by the antenna. In our deployment with the height difference shown in Fig. 6 (a),  $D_r = D(\theta_h + \pi/2) = a_r \sin^2(\theta_h + \pi/2)$ , where  $\theta_h$  is the depression angle. When the transmitter sways in the Y-Z plane,  $D_t = D(\pi - \theta_h - \theta_d) = a_t \sin^2(\pi - \theta_h - \theta_d)$ , where  $\theta_d$  is the directional angle between the transmitter antenna and the Y-axis. Then the Friis formula with polarization matching in Eq. 2 can be reformed as follows.

$$\begin{aligned} P_r(\theta_d, \theta_h) &= P_t \frac{\eta_t \eta_r \lambda^2}{(4\pi d)^2} D(\pi - \theta_h - \theta_d) D(\theta_h + \pi/2) \\ &= P_t \frac{\eta_t \eta_r \lambda^2}{(4\pi d)^2} \sin^2(\theta_h + \frac{\pi}{2}) \sin^2(\pi - \theta_d - \theta_h), \end{aligned} \quad (5)$$

We verify this model in a deployed environment. The height of the gateway is 6m, resulting in  $\theta_h = 1.15^\circ$ . For the convenience of recording ground-truth angles in 3D space, here we control the node attitude only in the Y-Z plane to verify the directivity loss. All the other settings are the same as the verification experiment in Section IV-A. The results are shown in Fig. 6(b), which fit well with our model. The RSS is much larger when tilting the same angle forwards to the receiver than backwards, which is consistent with the observations in Fig. 5. Due to the height difference, the transmitter antenna's maximum power points to the receiver at the attitudes satisfying  $\theta_d + \theta_h = 90^\circ$ . Tilting backwards has a chance to satisfy this condition. But keeping the antenna vertical upward in static scenarios can hardly meet this condition. This is why we observe RSS augments during our measurement study in Fig. 2.

### C. Link Model Based on Polarization and Directivity

Combining the polarization model and the directivity model, the Friis formula can be reformed as follows.

$$\begin{aligned} P_r(\theta_p, \theta_d, \theta_h) &= P_t \frac{\eta_t D_t \eta_r D_r \lambda^2}{(4\pi d)^2} p \\ &= P_0 \sin^2(\theta_p) \sin^2(\theta_h + \frac{\pi}{2}) \sin^2(\pi - \theta_d - \theta_h), \end{aligned} \quad (6)$$

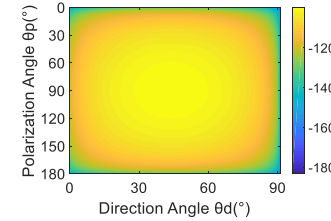


Fig. 7. Link Model based on polarization and directivity.

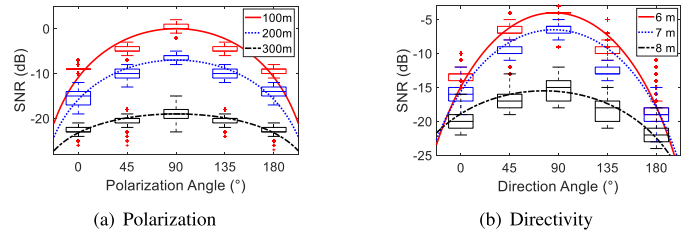


Fig. 8. The attitude impacts at different distances and height differences.

where  $P_0$  is the reference signal power that is related to the amplitude of the optimal received signal. Based on Eq. (6), we can obtain the link quality in terms of RSS at the attitude  $(\theta_p, \theta_d)$  as follows.

$$\begin{aligned} RSS(\theta_p, \theta_d, \theta_h) &= 10 \lg(P_r(\theta_p, \theta_d, \theta_h)) \\ &= RSS^* + RSS_{PL} + RSS_{DL} + RSS_{HL}, \end{aligned} \quad (7)$$

where  $RSS^*$  is the maximum available RSS at a fixed distance between transceivers, obtained when perfectly aligned.  $RSS_{PL}$ ,  $RSS_{DL}$ , and  $RSS_{HL}$  are the RSS losses caused by polarization, directivity, and height difference, which are:

$$\begin{aligned} RSS_{PL} &= 10 \lg(\sin^2(\theta_p)), \\ RSS_{DL} &= 10 \lg(\sin^2(\pi - \theta_h - \theta_d)), \\ RSS_{HL} &= 10 \lg(\sin^2(\theta_h + \pi/2)). \end{aligned} \quad (8)$$

Fig. 7 shows the link model based on polarization and directivity. We can find the theoretical RSS derived from our link model match the real received RSS.

We also verify the model at different distances and height differences between the transceivers. We set the Tx power to 4 dBm. When varying the distance from 100m to 300m, the height difference is fixed to 6m. And when varying the height difference from 6m to 8m, the distance between transceivers is fixed to 300m. The results in Fig. 8 show the Signal-to-Noise Ratio (SNR) which is calculated by the RSS divided by the noise floor. We present SNR to understand the link quality degradation more intuitively. We can find the measured SNR fits the theoretical model very well in Fig. 8. The results verify the effectiveness of the link model based on both polarization and directivity. From the results, we should notice that the model depends on the relative location of the transmitter. Hence, despite the small probability that the floating node drastically changes its position because of the anchors, we should consider the model update in the design.

Due to the continuity of physical motion, if there is bad transmission timing with poor link quality caused by attitude misalignment, there must be good transmission timing at the

aligned attitude. However, due to the wide range and dynamics of the floating node's attitude in 3D space, searching for the optimal attitude by probing transmissions at all the angles is infeasible. Obtaining the attitude-aware link model in practice and accordingly utilizing good transmission opportunities still need careful designs.

## V. DESIGN

In this section, based on the attitude-aware link model, we propose a novel channel access method called *PolarTracker* that schedules packets into attitude-aligned periods to improve the reliability of the floating LPWAN. We first present an overview of *PolarTracker* and then introduce the major modules.

### A. Overview

*PolarTracker*'s design goal is scheduling the channel access into the best-aligned periods to enhance the reliability of floating LPWAN. Even with the knowledge of the theoretical link model, obtaining the optimal fitting model and capturing the optimal attitude in practice is non-trivial. Most of the existing methods are probing-based methods that transmit a large number of probing packets to obtain fine-grained RSS measurements covering most of the targeted cases. However, such probing-based methods are not suitable for floating LoRa networks. The attitude of the floating node has a wide range in 3D space and changes quickly. The aligned period often lasts only hundreds of milliseconds at a time. But a probing packet in LoRa can take tens of milliseconds and even seconds, resulting in a too low probing rate to timely obtain enough representative RSS samples to fit the model. Besides, probing-based methods have a fundamental limitation of acquiring the attitude information. They solely rely on the measured link quality inside the network space but ignore the essential factors behind the phenomenon in physical space.

Instead of using the information in network space only, we utilize the physical attitude information to quickly establish the practical model for each floating node. We can learn from Eq. (7) that if we can obtain the attitude information ( $\theta_p, \theta_d$ ) and the corresponding RSS, we can obtain the fitting model by RSS at only a few different attitudes. Therefore, we propose leveraging the onboard Inertial Measurement Unit (IMU) to obtain the physical attitude information. Note that IMU is widely used in floating application systems to collect hydrologic data such as flow rate and flow direction [32], [33]. Hence, reusing the IMU information has no additional hardware or energy overhead. Even if the node has no IMU, adding an IMU has negligible hardware cost (\$10 for each) and very limited energy overhead.

Fig. 9 presents the overview of *PolarTracker*, which consists of three main modules: attitude recognition, link model establishment, and channel access. Initially, the *PolarTracker* client will use ALOHA in LoRaWAN to access the channel and record the IMU readings with the corresponding RSS. Since IMU provides only Euler angles, *PolarTracker* first estimates the antenna orientation to obtain the polarization angle  $\theta_p$  and the directivity angle  $\theta_d$ . Then the attitude ( $\theta_p^i, \theta_d^i$ )

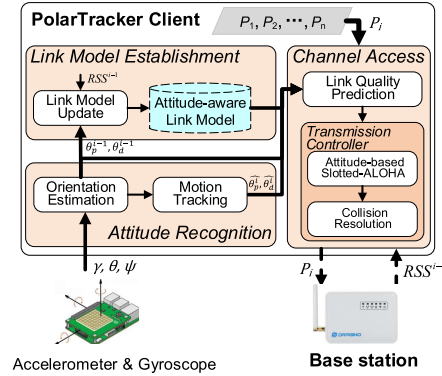


Fig. 9. Overview of *PolarTracker* design on a LoRa node.

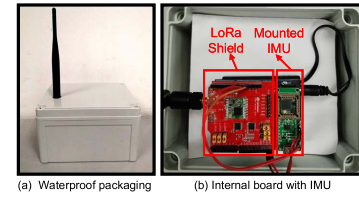


Fig. 10. The client mounted with IMU.

when transmitting packet  $i$ , along with the  $RSS^i$  piggybacked in the ACK from the gateway, is given to the link model establishment module. The model establishment module can estimate the parameters in the attitude-aware link model after accumulating a few measurements. After obtaining the model, the channel access comes into effect.

With the IMU data, we can track the node motion and predict node attitude in the following short time. By the current attitude and the predicted the next attitude, the link quality prediction module can determine the link quality at the next attitude based on the attitude-aware link model. If a significant RSS drop is predicted, *PolarTracker* will actively stop the packet transmission to avoid packet loss and resume the transmissions at the next alignment. To support concurrent access of multiple LoRa nodes with the same best-aligned period, the proposed attitude-based slotted-ALOHA protocol can adjust the transmission slots dynamically and adaptively according to the dynamic attitude. During the transmissions, the *PolarTracker* client can constantly update the model and track the dynamic alignment state.

### B. Attitude Recognition

To acquire the physical attitude information, we use the IMU fixed on the node board as shown in Fig. 10. Since the antenna is also fixed, its motion is the same as the node motion.

1) *Orientation Estimation*: As shown in Fig. 11, the IMU provides Euler angles,  $\gamma$ ,  $\theta$ , and  $\psi$ , based on its coordinate system  $ox_b y_b z_b$ . Even though the IMU's coordinate system may be different from the geographic coordinate system  $ox_n y_n z_n$ , their transformation relation is unchanged because the IMU is fixed on the board. We can easily obtain the transformation relation between two coordinate systems before deployment. For conciseness, without losing generality, we assume the two

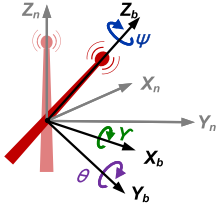


Fig. 11. Antenna sways in 3D space.

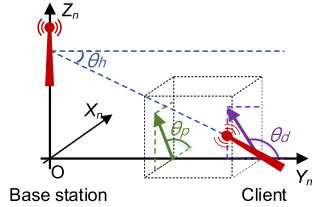


Fig. 12. Illustration of attitude recognition.

coordinate systems have been calibrated and consistent with each other in the following description.

When node swaying, the IMU coordinate relative to the geographical coordinate in terms of Euler angles can be expressed as:

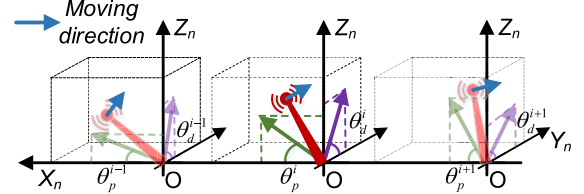
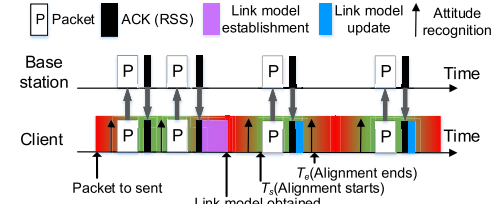
$$\begin{bmatrix} x_b \\ y_b \\ z_b \end{bmatrix} = C_n^b(\gamma, \theta, \psi) \begin{bmatrix} x_n \\ y_n \\ z_n \end{bmatrix} \quad (9)$$

where  $C_n^b(\gamma, \theta, \psi)$  is the Direction Cosine Matrix that indicates the relationship between two coordinate systems and can be expressed as follows [34].

$$C_n^b(\gamma, \theta, \psi) = \begin{pmatrix} \cos \psi & \sin \psi & 0 \\ -\sin \psi & \cos \psi & 0 \\ 0 & 0 & 1 \end{pmatrix} \begin{pmatrix} \cos \theta & 0 & \sin \theta \\ 0 & 1 & 0 \\ -\sin \theta & 0 & \cos \theta \end{pmatrix} \begin{pmatrix} 1 & 0 & 0 \\ 0 & \cos \gamma & -\sin \gamma \\ 0 & \sin \gamma & \cos \gamma \end{pmatrix} \quad (10)$$

Then we can obtain the coordinates of the antenna in the geographic coordinate system. As shown in Fig. 12, we can obtain the polarization angle  $\theta_p$  by projecting the antenna into the X-Z plane and calculating the angle between the projection and the positive X-axis base on the principle of space coordinate transformation. Similarly, we project the antenna into the Y-Z plane to obtain the directivity angle  $\theta_d$ .

**2) Motion Tracking:** Due to the software delay, starting the transmission after detecting a good attitude will lead to a delay of actual channel access, wasting the good transmission time. Hence, predicting the next attitude and loading packet just before the alignment is necessary. Though floating dynamics make the motion hard to model, we can track the short-term antenna motion due to the inertia and continuity of physical motions. In our design, the sampling rate of IMU is 200Hz. The continuous motion is divided into motion slots, each of which lasts 5ms. We use the most recent three slots to trace the motion direction and the angular velocity in the last slot as the angular velocity in the next slot. As shown in Fig. 13, *PolarTracker* uses the attitudes of  $i-1$  and  $i$  slots to predict the attitude of  $i+1$  slot. In this way, we can predict the following attitudes for the channel access that will be introduced in

Fig. 13. *PolarTracker* motion tracking.Fig. 14. *PolarTracker* establishes and updates the link model during transmission.

Section V-D. Note that the node will sway back after reaching the maximum magnitude, causing sudden direction changes. We can calibrate the predicted attitude by taking the remainder when the calculated results exceed the maximum historical magnitude.

### C. Attitude-Aware Link Model Establishment and Update

Based on the attitude  $(\hat{\theta}_p, \hat{\theta}_d)$  acquired by the attitude recognition module and the corresponding  $\hat{RSS}$ , we can estimate the parameters in Eq. (7) to obtain the link model for each floating node. The workflow in Fig. 14 presents how *PolarTracker* establishes and updates the attitude-aware link model. Initially, there is no information about the attitude and the link quality. Hence, *PolarTracker* follows LoRaWAN and adopts ALOHA to transmit the packets but records the corresponding attitudes when transmitting packets. We ask the gateway to piggyback the RSS of the received packets in the ACK messages. In this way, the *PolarTracker* client can collect the measured RSS value corresponding to the attitude at time  $i$ , i.e.,  $\{(\hat{\theta}_p^i, \hat{\theta}_d^i), \hat{RSS}^i\}$ . In Eq. (7) and Eq. (8), only two parameters,  $\theta_h$ , and  $RSS^*$ , are unknown. After accumulating several measurements, the attitude-aware link model for this floating node at this position can be established.

Due to the limited computing power of low-power LoRa nodes, solving the trigonometric and inverse trigonometric functions is infeasible. Hence, we calculate and store the values of the logarithmic sine function and the values of sine function from 0 to 90° with a step of 1° in advance. When calculating Eq. (8) and Eq. (10), *PolarTracker* directly queries the table using the angles. When we calculate the directivity loss, the directivity angle  $\theta_d$  will dominate and we can ignore the impact  $\theta_h$  because it will be much smaller than  $\theta_d$  in our targeted wide-area deployments where the communication distance is much longer than the height difference. Then *PolarTracker* will schedule and control the packets to be transmitted in the aligned periods. During the following transmissions, more observations of RSS at different attitudes can

be continuously accumulated and the model can be constantly updated to adapt to floating dynamics.

For floating LPWAN that have high deployment and maintaining cost, energy efficiency is crucial. Our model establishment and update method are light-weight and highly energy-efficient. The probing-based methods consume too much energy on transmitting probing packets. In LoRa, with a Tx power of 17 dBm, the current can be 87mA [7] and each packet can last for tens or even hundreds of milliseconds. Besides, due to the low achievable probing rate, blind probing has to cover multiple swaying rounds to obtain enough measurements at different attitudes to acquire the best link quality.

Different from the probing-based methods, we utilize the low-power IMU sensors to directly acquire the physical attitude information and obtain the RSS measurements from legacy data packets. The power consumption of the IMU sensor is only  $280\mu A$  in our current implementation, which is much lower than packet transmissions. Besides, if the application already has used IMU data, we can just reuse the data without extra overhead.

#### D. Channel Access

Different from LoRaWAN that accesses the channel immediately when there is a packet, *PolarTracker* proactively controls the channel access time to enhance the reliability. Without specific link quality, pinpointing the best channel access timing is challenging in practice. Hence, it is necessary to predict the link quality before transmission control.

1) *Link Quality Prediction*: The packet transmission has inevitable software delay, including the packet loading, radio state switching, etc. Therefore, if we make the decision after detecting a good-aligned attitude, the channel will be accessed with a non-negligible delay that wastes the valuable aligned period. *PolarTracker* integrates a link quality prediction component to predict the link quality at the next predicted attitude based on the link model and current attitude. The detailed procedure is shown in Algorithm 1, where  $RSS_{th}$  is a predefined RSS threshold difference between the reliable transmission and the maximum predicted by the model. If  $Flags_s$  is true, the packet will be sent in the next time slot, otherwise, it will not be sent. Firstly, we use the attitude information of the nearest slots to predict to track the node attitude and regard the angular velocity in the last slot as the angular velocity in the next slot (Line 1 to Line 2). With the predicted attitude at slot  $i + 1$ , the corresponding  $\hat{RSS}^{i+1}$  can be calculated (Line 3 to Line 6). When the node swaying causes misalignments, the predicted link quality gets worse. If the packet loss is suspected to happen, *PolarTracker* actively backs off to avoid the unreliable transmissions and keeps monitoring the attitude to discover the next alignment (Line 8 to Line 10). If the predicted link quality is getting better for reliable transmission, *PolarTracker* will schedule the transmission at the next attitude and start loading the next packet into the radio in advance (Line 12 to Line 14).

2) *Transmission Controller*: The goal of the transmission controller module is to schedule the channel access of packets into the aligned periods, as shown in Fig. 15. Specifically,

---

#### Algorithm 1 Link Quality Prediction

---

```

Input:  $(\theta_p^{i-1}, \theta_d^{i-1}), (\theta_p^i, \theta_d^i, RSS^i), RSS^*, \theta_h$ 
1  $\hat{\theta}_p^{i+1} = 2\theta_p^i - \theta_p^{i-1};$ 
2  $\hat{\theta}_d^{i+1} = 2\theta_d^i - \theta_d^{i-1};$ 
3  $\hat{RSS}_{PL}^{i+1} = 10 \lg(\sin^2(\theta_p^{i+1}));$ 
4  $\hat{RSS}_{DL}^{i+1} = 10 \lg(\sin^2(\pi - \theta_h - \theta_d^{i+1}));$ 
5  $\hat{RSS}_{HL}^{i+1} = 10 \lg(\sin^2(\theta_h + \pi/2));$ 
6  $\hat{RSS}(\theta_p^{i+1}, \theta_d^{i+1}, \theta_h) =$ 
    $RSS^* + \hat{RSS}_{PL}^{i+1} + \hat{RSS}_{DL}^{i+1} + \hat{RSS}_{HL}^{i+1};$ 
7 if  $|\hat{RSS}(\theta_p^{i+1}, \theta_d^{i+1}, \theta_h) - RSS^*| > RSS_{th}$  then
8   Backoff;
9    $Flags_s = FALSE;$ 
10  return  $(\hat{\theta}_p^{i+1}, \hat{\theta}_d^{i+1})$  and  $Flags_s$ 
11 else
12   Load packets;
13    $Flags_s = TRUE;$ 
14   return  $(\hat{\theta}_p^{i+1}, \hat{\theta}_d^{i+1}, \hat{RSS}^{i+1})$  and  $Flags_s$ 
15 end

```

---

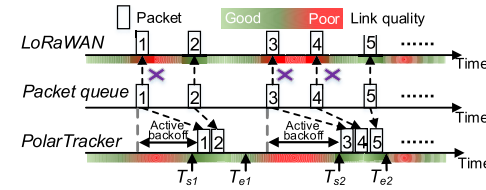


Fig. 15. *PolarTracker* proactively schedules the packets into attitude-aligned periods.

*PolarTracker* takes active backoff when predicting a bad aligned attitude. Once the channel quality at some time (such as  $T_{s1}$  and  $T_{s2}$ ) meets the transmission conditions according to the link prediction, *PolarTracker* loads the packet to transmit and does not end the transmission until all the packets to be transmitted are completed or the attitude aligned period ends.

However, in LoRaWAN, rather than solely communicating with a single client, the base station needs to connect extensive end devices. The challenge of multiple access is that there will be devastating collisions under high traffic loads, due to the adopted pure-ALOHA MAC protocol. One way to reduce collision, one might think, is using the slotted-ALOHA protocol, where the channel time is divided into slots and channel time is divided into slots, and all nodes transmit data only at the beginning of the slot. However, this fixed slots transmission becomes invalid over time, due to the dynamic attitude variation of nodes in aquatic environments. Even if the optimal transmission slot is initially allocated to each node, after working for a while, the allocated slot does not necessarily correspond to the attitude-aligned periods.

The attitude-based slotted-ALOHA protocol proposed in this paper can adjust the transmission slots dynamically and adaptively according to the dynamic attitude. Fig. 16 provides a comparison of LoRaWAN and *PolarTracker* with the attitude-based slotted-ALOHA protocol, where  $T$  is the scheduling period. Due to the dynamic attitude change, when LoRaWAN A and B send packets in the initially allocated

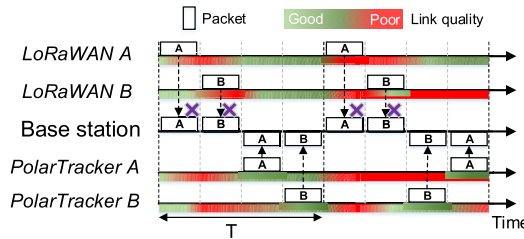


Fig. 16. A comparison of LoRaWAN with the slotted-ALOHA protocol and *PolarTracker* with the attitude-based slotted-ALOHA protocol.

slots, the base station fails to receive them. *PolarTracker* can make the node automatically adjust the transmission slot based on its attitude variation by the adaptive scheduler to improve communication reliability. This is inspired by the fact that the attitude variation of the client is the same over a short period of time.

*PolarTracker* adopts the guidance of the base station combined with the node attitude changing characteristics to achieve the adaptive scheduler. To synchronize the clients in the network, the base station is arranged to send beacons regularly. Once the beacon is received, the scheduling period begins for clients. Initially, all clients transmit slot request packets including client number and location according to their own attitude aligned periods. After receiving the packet, the base station extracts the client number and allocates a slot according to the received time and location. After all the allocation is successful, the base station broadcasts the time slot request response packet, the format of which includes the time slot length and the time slot number transmitted by each client.

However, there will be devastating collisions when multiple nodes with similar swaying behaviors select the same time slot for transmission. First of all, we should notice that since the best-aligned period is related to the location and the swaying behaviors, the collision probability is expected to be low. This is because the nodes in a floating network are expected to be sparsely deployed and they have completely different swaying behaviors. Therefore their attitude behaviors will be naturally different and they can locally choose a best-aligned time slot for transmission. Only when two nodes have similar attitude behaviors and link characteristics, their attitude-aligned periods can be similar and collision may happen.

*PolarTracker* utilizes the attitude variation characteristics and distance between clients and base station to deal with the collision. Fig. 17 shows an example of *PolarTracker*'s collision resolution, where nodes A and B are far away from the base station than nodes C and D. Once a collision is detected, the base station will send a broadcast packet to the node (A) far away from the base station to still select the original transmission slot, while the node (C) near the base station will switch to the adjacent idle slot for transmission because the channel quality of the adjacent time slot of the near node is better than that of the far node. Similarly, the collision solution between the newly added node (D) and the original node (B) also adopts the same strategy. If a node collides three times in succession, the transmission is deferred for a random interval. This random interval reduces the likelihood that two

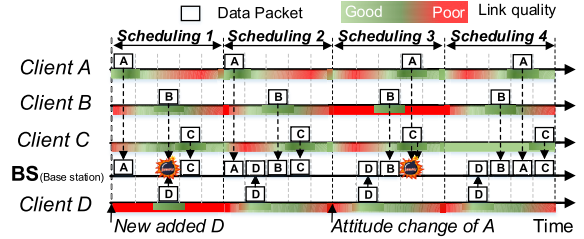


Fig. 17. *PolarTracker*'s collision resolution where D is newly added and the attitude-aligned periods of A and C are the same in scheduling 3 and 4, and B and D are the same in scheduling 1, 2, 3, and 4. Nodes A and B are far away from the base station than nodes C and D.

or more nodes waiting to transmit will simultaneously begin transmission, thus reducing the incidence of collision.

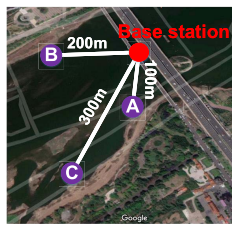
#### E. Overhead Analysis

For floating LPWAN that are difficult to deploy, low overhead is of great importance. Here, we discuss the overhead of *PolarTracker* from two aspects: computation overhead and communication overhead.

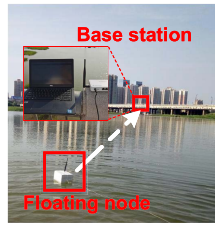
1) *Computation Overhead*: *PolarTracker* relies on attitude recognition and link model establishment to improve reliability. Hence, the major computation overhead of *PolarTracker* falls into the calculation of attitude and link model estimation. As described in Section V-B, *PolarTracker* needs to obtain the coordinates of the antenna in the geographic coordinate system by coordinate transformation and the attitude ( $\theta_p, \theta_d$ ) through space projection. Thus, the overhead of attitude calculation mainly comes from the acquisition of ( $\theta_p, \theta_d$ ) and the calculation is matrix multiplication whose computation overhead is  $O(3 \times 3 \times 1)$ . Note that the Euler angle is three-dimensional and *PolarTracker* stores the sine values from 0 to 90° with a step of 1° in advance. In addition, in the link model establishment, only two parameters need to be estimated and the process is a square operation whose computation overhead is  $O(n^2)$ . Therefore, the computational overhead of *PolarTracker* is acceptable.

2) *Communication Overhead*: To improve the client lifetime, the communication overhead of *PolarTracker* requires to be concerned. *PolarTracker* does not require the clients to transmit dedicated packets continuously but transmits data it needs to send itself and the RSS is obtained by piggybacking in the ACK from the base station. For the downlink, the nodes rarely miss the ACK from the gateway, because the gateway with a power supply usually adopts larger transmission power than the client node. Hence, the nodes receive the ACK even with attitude mismatch. But the floating nodes are often battery-powered and therefore have a smaller transmission power, which will be influenced by the attitude mismatch. Second, the gateway is usually static and higher than the water surface with a height. With such an angle of depression, the emission loss of the gateway transmission will not be high.

Moreover, during the transmission, *PolarTracker* just needs to monitor the attitude of the client in real-time based on IMU and only when a collision is detected, the base station needs to transfer broadcast packets to the clients to adjust



(a) Network deployment



(b) Experiment scene

Fig. 18. Experiment settings.

the transmission slots. Therefore, *PolarTracker* has limited communication overhead.

## VI. EVALUATION

We extensively evaluate *PolarTracker*'s performance in various real-world scenarios. First, we present the experiment settings and then show the evaluation results in detail.

### A. Experiment Setup

To evaluate *PolarTracker*, we implement and deploy a prototype system on commercial LoRa platforms with three clients and a gateway, as shown in Fig. 18(a). A Dragino LG01-P LoRa Device with HopeRF's RFM96W [35] is used as the base station. *PolarTracker* is implemented on the commercial Dragino Lora Shield [35] with Semtech SX1278. The gain of the antenna used in our prototype is 3 dBi. The network operates at the 433MHz frequency band and the length of the packet payload is 8 bytes. Unless explicitly specified, the parameters of LoRa nodes are set as:  $SF = 7$ ,  $BW = 250\text{kHz}$ , and  $CR = 4/5$  because of the distance limitation of our experimental environment to better test and compare the influence of polarization. In our experiments, we evaluate the performance of our method each method using 18000 packets. Note that *PolarTracker* can be compatible with the duty cycle limitation. With *PolarTracker*, a node operating in duty cycling mode can leverage the IMU component to construct the attitude-changing model. When there is a packet to transmit, we can quickly obtain the attitude-aware link model and track the aligned period for the transmission. Hence, for duty cycling end devices, *PolarTracker* can still help to improve transmission reliability. When evaluating point-to-point performance, we use client C. The IMU sampling rate is 200Hz. To compare with LoRaWAN, we also implement the ALOHA protocol on our prototype platforms. Fig. 18(b) shows the experiment scene.

### B. Real-World Performance in the Aquatic Environment

We first present an overview of the real-world performance of our deployed floating network in the aquatic environment. Fig. 19 shows the PRR and throughput of *PolarTracker* and LoRaWAN of the clients A, B, and C. For all three clients, *PolarTracker* achieves a better performance. From Fig. 19(a), we can find that the average PRR of *PolarTracker* of three clients are 99%, 94.7%, and 84.2%, while the average PRR of LoRaWAN is 91.4%, 75.1%, and 65.2%. *PolarTracker* is  $1.08\times, 1.26\times, 1.29\times$  better than LoRaWAN respectively.

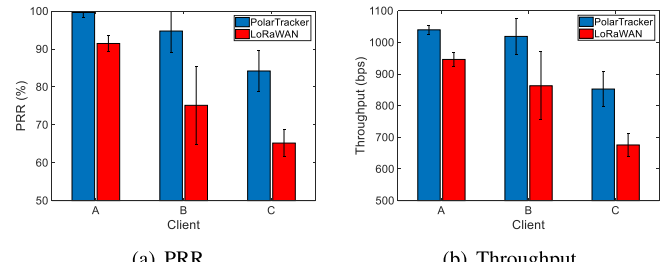


Fig. 19. The real-world performance in the aquatic environment.

The throughput is measured by the corrected received bits when transmitting at the highest data rate of LoRa. Similar improvements can be observed. The results demonstrate *PolarTracker* can indeed improve the reliability of floating networks in real-world aquatic environments. In the following, we will further evaluate *PolarTracker* in detail.

### C. Impact of LoRa Transmission Parameters

LoRa has multiple parameters that can influence reliability. Hence, we evaluate the performance of *PolarTracker* when LoRa uses different parameters to verify *PolarTracker* can improve the performance in different settings. For comparison, we also conduct the experiments using LoRaWAN in static and floating scenarios. During all the experiments, the distance between transceivers is consistent to keep fairness.

1) *Impact of Tx Power*: The foremost parameter is the Tx power that directly affects the RSS. Hence, we first study the performance of *PolarTracker* when varying the Tx power from 0 to 14 dBm. As shown in Fig. 20(a), *PolarTracker* can effectively improve the PRR to the level of LoRaWAN with the static scenario. Specifically, LoRaWAN can only obtain a PRR of 54.9% when Tx power is 2 dBm, while *PolarTracker* can achieve a PRR of 82.7% increasing by 50.6%, which is similar to the PRR when LoRaWAN uses a Tx power of 8 dBm. Besides, we find that due to the limitation of distance, the PRRs of different methods are similar when the transmission power is greater than 10 dBm. This is because, within the limited distance, the higher Tx power can make up the polarization loss. But this benefit performance comes at the cost of higher energy consumption. If the transmission distance is increased, the polarization loss will have significant effects on PRR and the advantage of *PolarTracker* will be more obvious. Moreover, we find that *PolarTracker* can achieve better performance than LoRaWAN in the static scenario because *PolarTracker* we can aggregate packets in the attitude alignment cycle for transmission.

2) *Impact of SF*: In LoRa, a chirp consists of a  $2^{SF}$  number of RF chips in a symbol window. Every increment of SF will double the transmission time of a chirp. Increasing SF will lower the sensitivity and have better reliability. Hence, we study the performance of three methods when SF varies from 7 to 12. The experimental results are shown in Fig. 20(b). As expected, with the increase of SF, PRR increases obviously. But at all settings, *PolarTracker* outperforms LoRaWAN. When the SF is 7, the PRR of *PolarTracker* reaches 80%, while the LoRaWAN is only 63.3%. What's worth noticing

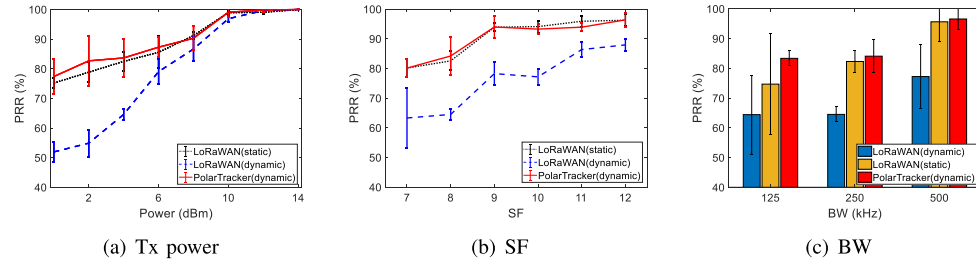


Fig. 20. Performance with different LoRa parameters.

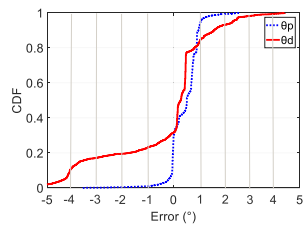


Fig. 21. The accuracy of attitude recognition.

is the PRR of *PolarTracker* with SF 8 is close to that of LoRaWAN with SF 11. It means *PolarTracker* can use a much lower SF for the floating nodes to obtain a similar PRR, which may bring a potential  $8\times$  data rate improvement.

3) *Impact of BW*: Similar to SF, BW is related to the data rate. We study the performance at commonly used BW 125, 250, and 500kHz. The experiment results are shown in Fig. 20(c). When using BW 125kHz, *PolarTracker* achieves the best PRR of 83.34%, which is 30% higher than the dynamic LoRaWAN. We can also find increasing bandwidth can improve reliability for all the methods. Based on our understanding, the reason behind this result is that the larger BW, the shorter time-on-air of a packet is, and the less affected by the dynamic attitude.

#### D. Performance of PolarTracker's Modules

1) *Accuracy of Attitude Recognition*: We first evaluate the accuracy of the attitude recognition module. We vary the antenna attitude at different angles from  $0^{\circ}$  to  $180^{\circ}$  in our lab and measure the calculation errors of  $\theta_p$  and  $\theta_d$  based on the IMU data. Fig. 21 shows the Cumulative Distribution Function (CDF) of the estimation errors of  $\theta_p$  and  $\theta_d$ . The average errors of  $\theta_p$  and  $\theta_d$  are  $0.44^{\circ}$  and  $0.36^{\circ}$  respectively. The accuracy is good enough for further link model establishment and transmission control.

2) *The Accuracy of Link Model*: Though our model can be calculated with only two RSS at different attitudes, more measurements can help improve the accuracy of parameter estimation. Hence, we study the estimation accuracy of  $RSS^*$  at a fixed height with varying the numbers of measurements in the deployed network. The parameter estimated by ten-minute measurements is regarded as the ground-truth. The average estimation errors using the different number of measurements are shown in Fig. 22. We can find that the error decreases when using more measurements, as expected. And using eight measurements is good enough to obtain the  $RSS^*$  estimation with an error of less than 1 dBm. Hence, in our current

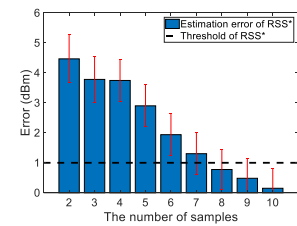
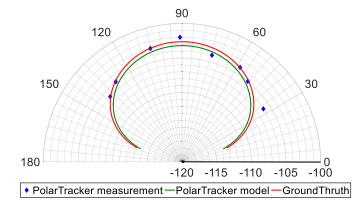


Fig. 22. The accuracy of the link model establishment.

Fig. 23. The fitting curve of *PolarTracker*.

implementation, we use eight measurements to establish the model. We also plot the curve of our fitting model obtained by eight measurements in the view of  $\theta_d$  in Fig. 23. Note that the link model is obtained by both  $\theta_d$  and  $\theta_p$ . We use the view of  $\theta_d$  only for display clearness. We can find the fitting curve is very close to the ground-truth. The results demonstrate that *PolarTracker* can quickly establish the link model based on only a few measurements.

3) *The Accuracy of Capturing the Aligned Attitude*: After obtaining the link model, we can capture the aligned attitude based on motion tracking and link quality prediction modules. As previously mentioned, channel probing based methods that transmit at the attitude with the best probed RSS are not accurate due to the low achievable probing rate. We compare the aligned attitude estimation accuracy of *PolarTracker* and the probing-based method based on 20 probing packets sent in one second. The deviations from the best-aligned attitude of the two methods are shown in Fig. 24. We can find that *PolarTracker* can capture an aligned attitude with less than  $1^{\circ}$  error for most of the cases. But the probing-based method with an error of nearly  $10^{\circ}$  cannot accurately capture the attitude.

4) *Impact of Antenna Gain*: Antenna gain is a comprehensive parameter to measure the energy conversion and directional characteristics. The higher the gain is the longer the wave can propagate at the same condition. To investigate the impact of antenna gain, we use three kinds of linearly polarized antennas with a gain of 3 dBi, 5 dBi, and 7 dBi

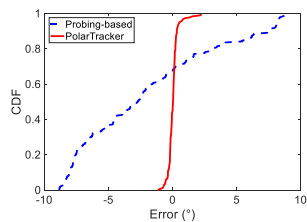


Fig. 24. The accuracy of capturing alignments.

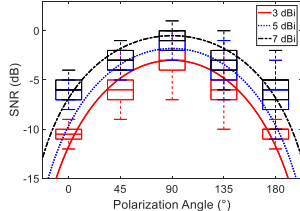


Fig. 25. Impact of antenna gain.

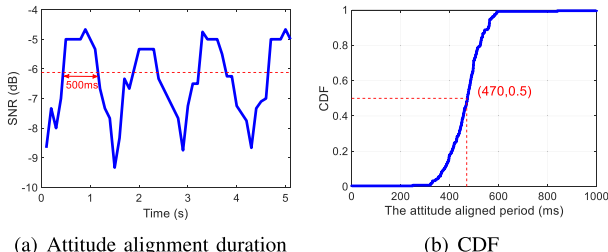


Fig. 26. The duration of attitude alignment.

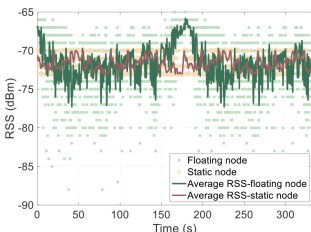


Fig. 27. The downlink RSS changes over time.

respectively. We rotate each antenna by the same angles and examine the polarization model. As shown in Fig. 25, the SNR at the same location increases with the increase of antenna gain, and the fitting polarization models for different antenna gains are different. The results show that the polarization model can be used for different antenna gains but the fitting parameters should be online decided to fit different antennas.

*5) The Duration of Attitude Alignment:* Attitude alignment duration corresponds to the time window of packet transmission. To show that the transmission can be completed within the attitude alignment time, we evaluate the attitude alignment duration. We show RSS changes within 5s in Fig. 26(a). For the first period, the alignment duration is about 500ms. Note that for *SF7*, the decodable SNR boundary of LoRa devices is  $-6.12\text{ dB}$  [36], [37]. A packet with a length of *8bytes* takes  $17.02\text{ms}$  to transmit when using *SF7* and  $BW = 250\text{kHz}$ . Fig. 26(b) shows the CDF of the alignment duration within half an hour. We can see that the median alignment period is  $470\text{ms}$ , and the minimum is greater than  $200\text{ms}$ , which is enough time to complete the transmission task.

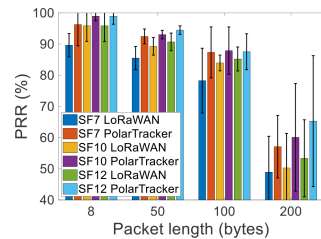


Fig. 28. Impact of packet length with different SF.

### E. Downlink RSS Variation

The reception of ACK from the gateway is related to *PolarTracker*'s performance. To illustrate that the nodes rarely miss the ACK, Fig. 27 shows the downlink RSS variation over time at a distance of  $300m$ . We can see the average RSS of the downlink is  $37\text{ dB}$  higher than the average RSS of the uplink in Fig. 2(c) because the gateway adopts larger transmission power. The minimum received RSS of the floating node is  $-88\text{ dBm}$ , which is enough for the node to capture ACK.

### F. Impact of Packet Length With Different SF

The time-on-air of a packet of a LoRa packet is related to SF, BW, and packet length. To investigate the impact of different time-on-air, we evaluate the performance of *PolarTracker* and LoRaWAN when the payload length varies from *8bytes* to *200bytes* at SF7, SF10, and SF12. From Fig. 28, the PRR of *PolarTracker* decreases with the increase of payload length because a large payload length will increase the probability that a packet is transmitted out of the aligned duration. Specifically, when the payload length is *200bytes* at SF7, the PRR is only  $57\%$ . Although the PRR of *PolarTracker* decreases with the increase of payload length, the performance is better than LoRaWAN because the transmission in the attitude alignment duration gives more chance to receive the packet.

### G. Comparison With the Retransmission Scheme

Retransmission is a simple method that resends the lost packets, identical to automatic repeat request (ARQ). But blind retransmissions in floating LPWAN cost too much energy. We compare *PolarTracker* with LoRaWAN augmented with ARQ when the client has different packet rates. The results are shown in Fig. 29. We can find that retransmission can also improve the PRR, obtaining a similar PRR to *PolarTracker*. But the retransmission scheme is to gain the benefit of PRR at the expense of energy consumption. From the results in Fig. 29(b), we can find a large number of retransmissions are needed to obtain the PRR improvements. But *PolarTracker* only needs to transmit once. For the energy-hungry floating LPWAN, the energy-consuming retransmission scheme is unfavored.

### H. Comparison With the Circularly Polarized Antenna

According to antenna theory, the attitude of linear polarization antenna can affect the efficiency of signal reception, while circularly polarized antenna can receive linearly polarized electromagnetic waves in any polarization direction as shown

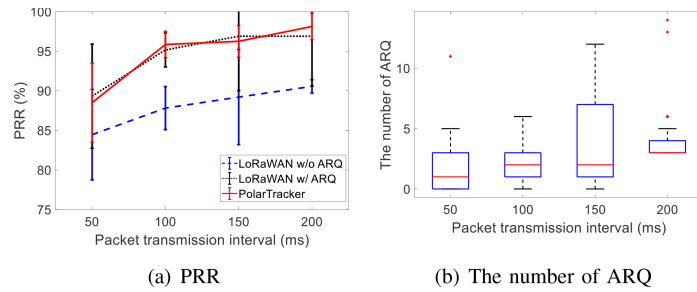


Fig. 29. Comparison with the retransmission scheme.

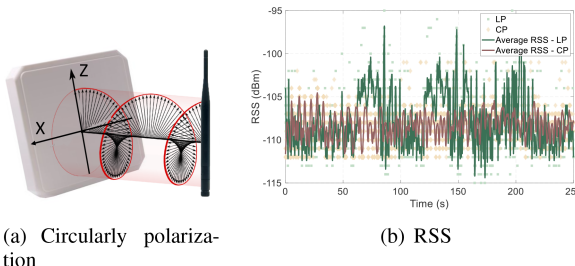


Fig. 30. Comparison of circularly polarized (CP) and linearly polarized (LP) receiving antenna.

in Fig. 30(a). Does this mean that the circularly polarized antenna can solve the problem caused by the polarization mismatch? To answer this question, we explore the performance of the receiving antennas with linearly and circularly polarized in the case of random rotation of the transmitting antenna. Fig. 30(b) shows RSS received by circularly polarized (CP) and linearly polarized (LP) receiving antennas. We can find that the RSS with circularly polarized antenna is relatively stable, and the RSS with linearly polarized antenna has much larger variations. But we can find that LP can obtain much higher RSSI than CP in many cases. This is because though CP antennas avoid the RSS variations caused by polarization mismatch, they also miss the opportunities to obtain higher RSS during the aligned polarization period. But our method can capture these opportunities and allow the floating nodes to access the channel during the aligned periods. Besides, due to the packaging size and shape, a CP antenna is less suitable for floating IoT devices than an LP antenna.

### I. Energy Consumption

For low-power devices, energy efficiency is of great importance. *PolarTracker* with fewer retransmissions can schedule the transmissions into the aligned periods with better link quality, while for LoRaWAN with ALOHA, the increased number of retransmissions due to lower PRR makes its energy consumption higher. We compare the energy consumption of *PolarTracker* and LoRaWAN with the retransmission scheme in half an hour when Tx power is 4 dBm. The current in the receiving standby state of the *PolarTracker* is 10.3mA and the current of IMU is only 280 $\mu$ A [38]. We measure the energy consumption in varying packet transmission intervals. Note that the energy consumption of LoRaWAN consists of the overhead of standby and packet transmission and *PolarTracker* needs to add the energy consumption of IMU on this basis.

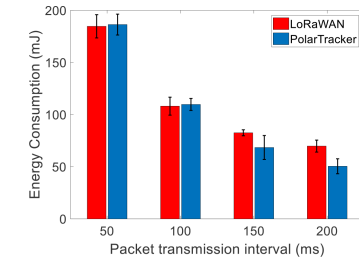


Fig. 31. Energy consumption.

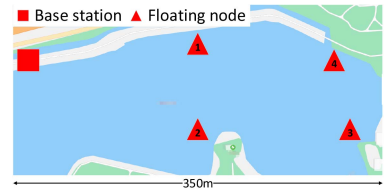


Fig. 32. Experiment scene of outdoor real LoRa network.

From the results in Fig. 31, we can find that the energy consumption of *PolarTracker* is significantly lower than that of LoRaWAN when the packet transmission interval is greater than 100ms. Therefore, for low duty-cycle floating LPWAN, the energy efficiency can be improved because of avoidance of unnecessary transmission.

### J. Performance of the Attitude-Based MAC Protocol

To demonstrate the effectiveness of attitude-based MAC protocol, we evaluate its performance in a real network deployed in the aquatic environment. As illustrated in Fig. 32, the outdoor LoRa network consists of 4 floating nodes with different distances from the base station. The PRR results are shown in Fig. 33(a) and (b). The PRR of *PolarTracker* is better than the default LoRaWAN, especially for nodes far away from the base station. For node 4, the average PRR of LoRaWAN and *PolarTracker* are 67.4% and 95.8%.

In the experiment, we also evaluate *PolarTracker*'s performance as the number of active nodes increases in the LoRa network. The results are shown in Fig. 33(c) and (d). For LoRaWAN ignoring the node attitude, the PRR decreases as the network scales, while the PRR of *PolarTracker* is no less than 95%. Besides, the PRR difference between LoRaWAN and *PolarTracker* also increases with the increase of the number of active nodes. We also compare the throughput when increasing the number of active nodes. The results are shown in Fig. 33(d). The network throughput of *PolarTracker* is about

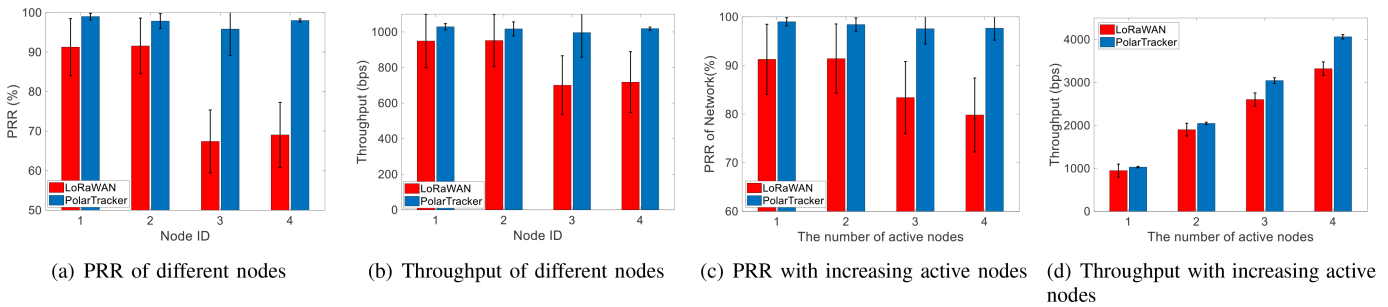


Fig. 33. Performance of the attitude-based MAC protocol.

1.21 $\times$  than that of LoRaWAN when all deployed nodes are simultaneously active.

## VII. CONCLUSION

In this paper, we propose *PolarTracker*, a novel attitude-aware channel access method dedicated to the floating LPWAN. We theoretically establish an attitude-aware link model that quantitatively describes the relationship between the attitude of a floating node and its link quality. Instead of using only in-network probed information, *PolarTracker* also leverages the onboard IMU to directly acquire the physical attitude information and quickly obtain the practical link model with only a few measurements. *PolarTracker* tracks the node attitude alignment state and actively schedules the packets to access the channel during the aligned periods with better link qualities. An attitude-based slotted-ALOHA protocol is proposed to support concurrent access of multiple LoRa nodes with the same best-aligned period. The extensive experimental results demonstrate the efficiency of *PolarTracker*. In real-world deployment in aquatic environments, *PolarTracker* can improve the PRR by 50.6%, compared with LoRaWAN with ALOHA.

## REFERENCES

- [1] N. Sornin, M. Luis, T. Eirich, T. Kramp, and O. Herset, “LoRaWAN specification,” LoRaWAN Specification v1.0.2, LoRa Alliance, Tech. Rep. v1.0.2, 2016.
- [2] M. Chen, Y. Miao, Y. Hao, and K. Hwang, “Narrow band Internet of Things,” *IEEE Access*, vol. 5, pp. 20557–20577, 2017.
- [3] L. Parri, S. Parrino, G. Peruzzi, and A. Pozzebon, “A LoRaWAN network infrastructure for the remote monitoring of offshore sea farms,” in *Proc. IEEE Int. Instrum. Meas. Technol. Conf.*, May 2020, pp. 1–6.
- [4] P. S. Dehda, S. Jayram, A. M. Abu-Mahfouz, and K. Ouahada, “A sea rescue operation system based on LoRa,” in *Proc. Int. Conf. Adv. Big Data, Comput. Data Commun. Syst.*, Aug. 2019, pp. 1–6.
- [5] W. Du, Z. Xing, M. Li, B. He, L. H. C. Chua, and H. Miao, “Optimal sensor placement and measurement of wind for water quality studies in urban reservoirs,” in *Proc. 13th Int. Symp. Inf. Process. Sensor Netw.*, Apr. 2014, pp. 167–178.
- [6] J. Cecilio, P. M. Ferreira, and A. Casimiro, “Evaluation of LoRa technology in flooding prevention scenarios,” *Sensors*, vol. 20, no. 14, p. 4034, Jul. 2020.
- [7] SX1278. (2020). *Datasheet SX1276/77/78/79*. [Online]. Available: <https://semtech.my.salesforce.com>
- [8] F. Cuomo, M. Campo, A. Caponi, G. Bianchi, G. Rossini, and P. Pisani, “EXPLoRa: Extending the performance of LoRa by suitable spreading factor allocations,” in *Proc. IEEE 13th Int. Conf. Wireless Mobile Comput., Netw. Commun.*, Oct. 2017, pp. 1–8.
- [9] J. C. Liando, A. Gamage, A. W. Tengoutius, and M. Li, “Known and unknown facts of LoRa: Experiences from a large-scale measurement study,” *ACM Trans. Sensor Netw.*, vol. 15, no. 2, pp. 1–35, Feb. 2019.
- [10] B. Paul, “A novel mathematical model to evaluate the impact of packet retransmissions in LoRaWAN,” *IEEE Sensors Lett.*, vol. 4, no. 5, pp. 1–4, May 2020.
- [11] R. Choi, S. Lee, and S. Lee, “Reliability improvement of LoRa with ARQ and relay node,” *Symmetry*, vol. 12, no. 4, p. 552, Apr. 2020.
- [12] H. Li, Y. Gao, W. Dong, and C. Chen, “Bound-based network tomography for inferring interesting link metrics,” in *Proc. IEEE Conf. Comput. Commun.*, Jul. 2020, pp. 1588–1597.
- [13] W. Dong, C. Cao, X. Zhang, and Y. Gao, “Understanding path reconstruction algorithms in multihop wireless networks,” *IEEE/ACM Trans. Netw.*, vol. 27, no. 1, pp. 1–14, Feb. 2019.
- [14] Y. Peng *et al.*, “PLoRa: A passive long-range data network from ambient LoRa transmissions,” in *Proc. Conf. ACM Special Interest Group Data Commun.*, Aug. 2018, pp. 147–160.
- [15] X. Xia, Y. Zheng, and T. Gu, “LiteNap: Downclocking LoRa reception,” in *Proc. IEEE Conf. Comput. Commun.*, Jul. 2020, pp. 2321–2330.
- [16] G. Guan, B. Li, Y. Gao, Y. Zhang, J. Bu, and W. Dong, “TinyLink 2.0: Integrating device, cloud, and client development for IoT applications,” in *Proc. 26th Annu. Int. Conf. Mobile Comput. Netw.*, Apr. 2020, pp. 1–13.
- [17] G. Chen, W. Dong, Z. Zhao, and T. Gu, “Towards accurate corruption estimation in ZigBee under cross-technology interference,” in *Proc. IEEE 37th Int. Conf. Distrib. Comput. Syst.*, Jun. 2017, pp. 425–435.
- [18] K. Liu *et al.*, “Oceansense: Monitoring the sea with wireless sensor networks,” *ACM SIGMOBILE Mobile Comput. Commun. Rev.*, vol. 14, no. 2, pp. 7–9, Sep. 2010.
- [19] H. Ferreira *et al.*, “Autonomous systems in remote areas of the ocean using BLUECOM+ communication network,” in *Proc. OCEANS Anchorage*, 2017, pp. 1–6.
- [20] B. Reinders, W. Meert, and S. Pollin, “Power and spreading factor control in low power wide area networks,” in *Proc. IEEE Int. Conf. Commun. (ICC)*, May 2017, pp. 1–6.
- [21] A. Gamage, J. C. Liando, C. Gu, R. Tan, and M. Li, “LMAC: Efficient carrier-sense multiple access for LoRa,” in *Proc. 26th Annu. Int. Conf. Mobile Comput. Netw.*, Sep. 2020, pp. 1–13.
- [22] C. Wang, Y. Chen, and S. Yang, “Dual-band dual-polarized antenna array with flat-top and sharp cutoff radiation patterns for 2G/3G/LTE cellular bands,” *IEEE Trans. Antennas Propag.*, vol. 66, no. 11, pp. 5907–5917, Nov. 2018.
- [23] S. Wen, Y. Xu, and Y. Dong, “A low-profile dual-polarized omnidirectional antenna for LTE base station applications,” *IEEE Trans. Antennas Propag.*, vol. 69, no. 9, pp. 5974–5979, Sep. 2021.
- [24] Y. Pan, Y. Dong, and Z. Wang, “Circularly polarized V-shaped patch antenna for RFID application,” in *Proc. IEEE Int. Symp. Antennas Propag. USNC-URSI Radio Sci. Meeting*, Jul. 2019, pp. 1893–1894.
- [25] A. Mikhailovskaya *et al.*, “Omnidirectional miniature RFID tag,” *Appl. Phys. Lett.*, vol. 119, no. 3, Jul. 2021, Art. no. 033503.
- [26] Z. Wang, M. Xu, N. Ye, H. Huang, R. Wang, and F. Xiao, “RF-mirror: Mitigating mutual coupling interference in two-tag array labeled RFID systems,” in *Proc. 17th Annu. IEEE Int. Conf. Sens., Commun., Netw. (SECON)*, Jun. 2020, pp. 1–9.
- [27] LoRa Alliance, “White paper: A technical overview of LoRa and LoRaWAN,” CA, USA, White Paper, 2015.
- [28] N. Abramson, “The Aloha system: Final technical report,” Hawaii Univ. Honolulu, Honolulu, HI, USA, 1974.
- [29] R. C. Johnson and H. Jasik, *Antenna Engineering Handbook*. New York, NY, USA: McGraw-Hill, 1984.
- [30] C. A. Balanis, *Antenna Theory: Analysis and Design*. Hoboken, NJ, USA: Wiley, 2016.

- [31] L. Shangguan and K. Jamieson, "Leveraging electromagnetic polarization in a two-antenna whiteboard in the air," in *Proc. 12th Int. Conf. Emerg. Netw. Exp. Technol.*, Dec. 2016, pp. 443–456.
- [32] J.-H. Chen, S.-C. Lee, and D. B. DeBra, "Gyroscope free strapdown inertial measurement unit by six linear accelerometers," *J. Guid., Control, Dyn.*, vol. 17, no. 2, pp. 286–290, 1994.
- [33] G. Dissanayake, S. Sukkarieh, E. Nebot, and H. Durrant-Whyte, "The aiding of a low-cost strapdown inertial measurement unit using vehicle model constraints for land vehicle applications," *IEEE Trans. Robot. Autom.*, vol. 17, no. 5, pp. 731–747, Oct. 2001.
- [34] A. Mokhtari and A. Benallegue, "Dynamic feedback controller of Euler angles and wind parameters estimation for a quadrotor unmanned aerial vehicle," in *Proc. IEEE Int. Conf. Robot. Autom.*, Jul. 2004, pp. 2359–2366.
- [35] Queensland University of Technology Brisbane. *LG01 LoRa Gateway User Manual*. Accessed: Aug. 1, 2020. [Online]. Available: <https://www.dragino.com>
- [36] Y. Li, J. Yang, and J. Wang, "DyLoRa: Towards energy efficient dynamic LoRa transmission control," in *Proc. IEEE Conf. Comput. Commun.*, Jul. 2020, pp. 2312–2320.
- [37] T. Elshabrawy and J. Robert, "Closed-form approximation of LoRa modulation BER performance," *IEEE Commun. Lett.*, vol. 22, no. 9, pp. 1778–1781, Sep. 2018.
- [38] Asahi Kasei Microdevices Corporation. *AK8963 3-Axis Electronic Compass*. Accessed: Aug. 1, 2020. [Online]. Available: <https://datasheetspdf.com/datasheet/ak8963.html>



**Yuting Wang** received the B.E. and M.A. degrees from the Henan University of Science and Technology, China, in 2015 and 2018, respectively. She is currently pursuing the Ph.D. degree with the School of Computer Science and the Beijing Key Laboratory of Intelligent Telecommunications Software and Multimedia, Beijing University of Posts and Telecommunications, China. Her research interests include the Internet of Things and wireless networks.



**Xiaolong Zheng** (Member, IEEE) received the B.E. degree from the Dalian University of Technology, China, in 2011, and the Ph.D. degree from The Hong Kong University of Science and Technology in 2015. He is currently an Associate Professor with the School of Computer Science and the Beijing Key Laboratory of Intelligent Telecommunications Software and Multimedia, Beijing University of Posts and Telecommunications, China. His research interests include the Internet of Things, wireless networks, and ubiquitous computing.



**Liang Liu** (Member, IEEE) received the B.S. degree from the Department of Computer Science and Technology, South China University of Technology, Guangzhou, China, in 2004, and the Ph.D. degree from the School of Computer Science, Beijing University of Posts and Telecommunications, Beijing, China, in 2009.

He was a Visiting Ph.D. Student with the Networking and Information Systems Laboratory, Texas A&M University, College Station, TX, USA, from 2007 to 2008. He is currently a Professor with the Beijing Key Laboratory of Intelligent Telecommunications Software and Multimedia, and the Dean of the School of Artificial Intelligence, Beijing University of Posts and Telecommunications. He has published over 170 articles. His current research interests include the Internet of Things and intelligent sensing technologies.



**Huadong Ma** (Fellow, IEEE) received the B.S. degree in mathematics from Henan Normal University, Xinxiang, China, in 1984, the M.S. degree in computer science from the Shenyang Institute of Computing Technology, Chinese Academy of Sciences, Beijing, China, in 1990, and the Ph.D. degree in computer science from the Institute of Computing Technology, Chinese Academy of Sciences, in 1995.

From 1999 to 2000, he held a visiting position at the University of Michigan, Ann Arbor, MI, USA. He is currently a Professor with the School of Computer Science, Beijing University of Posts and Telecommunications (BUPT), China. He has published more than 300 papers in prestigious journals (such as ACM/IEEE TRANSACTIONS) or conferences (such as ACM SIGCOMM, ACM MobiCom/MM, and IEEE INFOCOM) and five books. His current research interests include the Internet of Things and sensor networks, and multimedia computing.

Dr. Ma received the First Class Prize of the Natural Science Award of the Ministry of Education, China, in 2017. He received the 2019 Prize Paper Award of IEEE TRANSACTIONS ON MULTIMEDIA, the 2018 Best Paper Award from IEEE MULTIMEDIA, the Best Paper Award in IEEE ICPADS2010, and the Best Student Paper Award in IEEE ICME2016 for his coauthored papers. He received the National Funds for Distinguished Young Scientists in 2009. He also serves as the Chair for ACM SIGMOBILE China. He was/is an Editorial Board Member of the IEEE TRANSACTIONS ON MULTIMEDIA, IEEE INTERNET OF THINGS JOURNAL, ACM Transactions on Internet of Things, and *Multimedia Tools and Applications*.